Journal of Nuclear Materials 396 (2010) 234–239

Contents lists available at ScienceDirect

Journal of Nuclear Materials

journal homepage: www.elsevier.com/locate/jnucmat

# Transmission electron microscopy characterization of irradiated U–7Mo/Al–2Si dispersion fuel

J. Gan [a,*], D.D. Keiser Jr. [a], D.M. Wachs [a], A.B. Robinson [a], B.D. Miller [b], T.R. Allen [b]

[a] Nuclear Fuels and Materials Division, Idaho National Laboratory, P.O. Box 1625, Idaho Falls, ID 83403, USA
[b] University of Wisconsin, Madison, WI 53706, USA

ARTICLE INFO

*Article history:*
Received 23 June 2009
Accepted 18 November 2009

ABSTRACT

The plate-type dispersion fuels, with the atomized U(Mo) fuel particles dispersed in the Al or Al alloy matrix, are being developed for use in research and test reactors worldwide. It is found that the irradiation performance of a plate-type dispersion fuel depends on the radiation stability of the various phases in a fuel plate. Transmission electron microscopy was performed on a sample (peak fuel mid-plane temperature ~109 °C and fission density ~$4.5 \times 10^{27}$ f m$^{-3}$) taken from an irradiated U–7Mo dispersion fuel plate with Al–2Si alloy matrix to investigate the role of Si addition in the matrix on the radiation stability of the phase(s) in the U–7Mo fuel/matrix interaction layer. A similar interaction layer that forms in irradiated U–7Mo dispersion fuels with pure Al matrix has been found to exhibit poor irradiation stability, likely as a result of poor fission gas retention. The interaction layer for both U–7Mo/Al–2Si and U–7Mo/Al fuels is observed to be amorphous. However, unlike the latter, the amorphous layer for the former was found to effectively retain fission gases in areas with high Si concentration. When the Si concentration becomes relatively low, the fission gas bubbles agglomerate into fewer large pores. Within the U–7Mo fuel particles, a bubble superlattice ordered as fcc structure and oriented parallel to the bcc metal lattice was observed where the average bubble size and the superlattice constant are 3.5 nm and 11.5 nm, respectively. The estimated fission gas inventory in the bubble superlattice correlates well with the fission density in the fuel.



## 1. Introduction

Plate-type dispersion fuels are widely used for the research and test reactors. The fuel plate, typically about 1.5 mm thick, has three layers with each at a thickness of approximately 0.50 mm. The top and bottom layers are the cladding made of 6061 Al. In a low-enriched uranium (LEU) U–Mo fuel being developed to replace high-enriched uranium (HEU), the middle layer has atomized U(Mo) fuel particles dispersed in a matrix of pure Al or Al alloy. A schematic cutoff view of the dispersion fuel plate is shown in Fig. 1. It has been shown that γ-U (bcc crystal structure) based fuels are more stable than α-U (orthorhombic crystal structure) based fuels under irradiation. Uranium alloying with 7–10 wt% Mo has been shown to be effective in stabilizing γ-phase and improving fuel performance [1,2]. During operation in a reactor, the fuel plate is in contact with coolant water at coolant temperatures typically around 65 °C [3].

The development of U–Mo dispersion fuels is a part of a global effort on nuclear non-proliferation and these LEU fuels are being developed by the US Reduced Enrichment for Research and Test Reactors (RERTR) program [4]. A big part of the development of LEU fuels has involved using the Advanced Test Reactor (ATR) at Idaho National Laboratory (INL) to test different fuel types to investigate irradiation performance. The RERTR-6 experiment with 19.7% enriched uranium fuels was the first to test dispersion fuels with Si-containing Al alloy matrices [5]. Si is added to the matrix of a U–Mo dispersion fuel to enable the formation of a stable U–Mo/matrix interaction layer that is expected to behave well during irradiation. A similar interaction layer in U–7Mo dispersion fuels with only Al as the matrix does not exhibit good irradiation performance [6]. Transmission electron microscopy (TEM) characterization of the layers in an irradiated U–7Mo/Al dispersion fuel showed that the interaction layer that was present around the U–7Mo fuel particles was amorphous without stable gas bubbles [7]. Instead, the fission gases migrated to the interaction layer/matrix interface, where they can develop into relatively large pores that could link and cause fuel plate failure. By adding Si to the matrix of a U–Mo dispersion fuel, it is predicted that a more stable interaction layer will develop that can better accommodate fission gases [8].

* Corresponding author. Address: Nuclear Fuels and Materials Division, Idaho National Laboratory, P.O. Box 1625, Idaho Falls, ID 83415-6188, USA. Tel.: +1 208 533 7385; fax: +1 208 533 7863.
*E-mail address:* Jian.Gan@inl.gov (J. Gan).

0022-3115/$ - see front matter © 2009 Elsevier B.V. All rights reserved.
doi:10.1016/j.jnucmat.2009.11.015

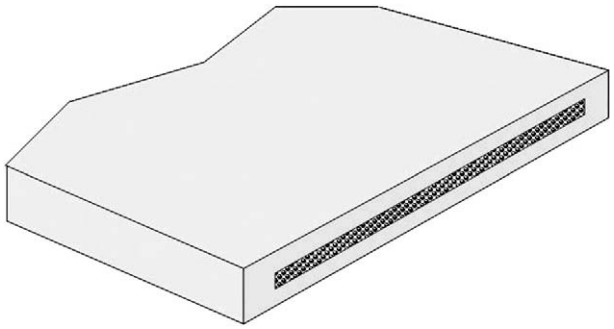

**Fig. 1.** A schematic of cutoff view of a dispersion fuel plate showing U(Mo) fuel particles dispersed in Al alloy matrix in the middle layer.

In order to investigate the performance of U–7Mo/matrix interaction layers in an irradiated U–7Mo/Al–2Si fuel plate, TEM characterization was performed on a sample taken from fuel plate R2R010, which was irradiated in ATR as part of the RERTR-6 experiment. Note that the fission density in this sample was three times that reported by Van den Berghe et al. [7]. Characterization of this same fuel plate using scanning electron microscopy (SEM) was reported by Keiser et al. [9]. This paper will discuss the findings of TEM investigation in terms of the observed microstructures of the irradiated U–7Mo particles and U–7Mo/matrix interaction layer. Behavior of the fission gases within the U–7Mo and interaction layers will also be described.

## 2. Experiment

Since the TEM sample was prepared from a small punching out of a fuel plate, it is important to provide the irradiation conditions for the plate. For the RERTR-6 experiment, fuel plates were tested to medium burnup under moderate flux and temperature conditions. These plates were positioned edge-on with respect to the core, and as a result had a steep neutron flux gradient across the widths of the fuel plates. For plate R2R010, the calculated peak temperature at fuel plate mid-plane was 109 °C as determined using the PLATE fuel performance code [10]. The plate average fission density was $3.2 \times 10^{27}$ f m$^{-3}$, the average fission rate was $2.7 \times 10^{20}$ f m$^{-3}$ s$^{-1}$; and the peak heat flux for the entire plate was $1.48 \times 10^{6}$ W m$^{-2}$.

A TEM sample was prepared from a 1.0-mm-diameter, cylindrical sample (length ~1.4 mm) taken from the high-flux side of the fuel plate in a hot cell by a punching method described elsewhere [11]. The local irradiation conditions for the sample taken from this side of R2R010 resulted in average fission density, average fission rate, and peak heat flux values of approximately $4.5 \times 10^{27}$ f m$^{-3}$, $3.8 \times 10^{20}$ f m$^{-3}$ s$^{-1}$, and $1.48 \times 10^{6}$ W m$^{-2}$, respectively [9]. In INL's Electron Microscopy Laboratory, the sample was glued inside a 3.0-mm-diameter Mo ring using epoxy and mechanically wet-polished from both sides down to ~100 μm thickness inside a glove-box. The disc sample was followed by jet electropoling and finally ion polishing to perforation. The finished sample was then characterized using a JEOL2010 TEM operated at 200 kV.

## 3. Results

Optical metallography images from a full transverse cross section taken at the mid-plane of R2R010 fuel plate are presented in Fig. 2 to show the overall as-irradiated microstructure from which the TEM sample was produced. From higher magnification images, it can be seen that narrow interaction layers are present around the U–7Mo particles. The results from high resolution TEM analysis are presented beginning with characterization of U–7Mo fuel particles, followed by that of interaction layers.

### 3.1. Characterization of the U–7Mo fuel particles

When producing TEM images of the U–7Mo particles, it was found that in some cases oxide particles were present on the fuel particles, due to the exposure of the sample to air before it could be inserted into the TEM. However, many areas of the U–7Mo particles were found where surface oxidation was not a problem and high-quality TEM images could be obtained. It was observed that the U–7Mo fuel particle remains crystalline gamma phase (bcc) after irradiation. TEM bright field images and the selected-area diffraction (SAD) pattern of a U–7Mo particle in the R2R010 sample are presented in Fig. 3, showing the bubble superlattice at different magnifications with bcc metal oriented at zone [0 1 1]. A slightly under-focus in the bright filed imaging enhances the contrast of these three-dimensionally-ordered bubbles. The average size and its standard deviation of the fission gas bubbles were measured to be ~3.5 ± 0.4 nm. The plane spacing for "A" and "B" for bubble superlattice measured from bright filed image are 5.75 nm and 6.55 nm, respectively. The corresponding plane spacing estimated from the satellite spots are 5.88 nm and 6.39, respectively. The plane spacing measured from bright field image and the satellite spots are consistent within less than 2.5% relative error. Bubble superlattice is observed as a general microstructural feature in all transparent areas in U–7Mo fuel particles. The oxide rings in the

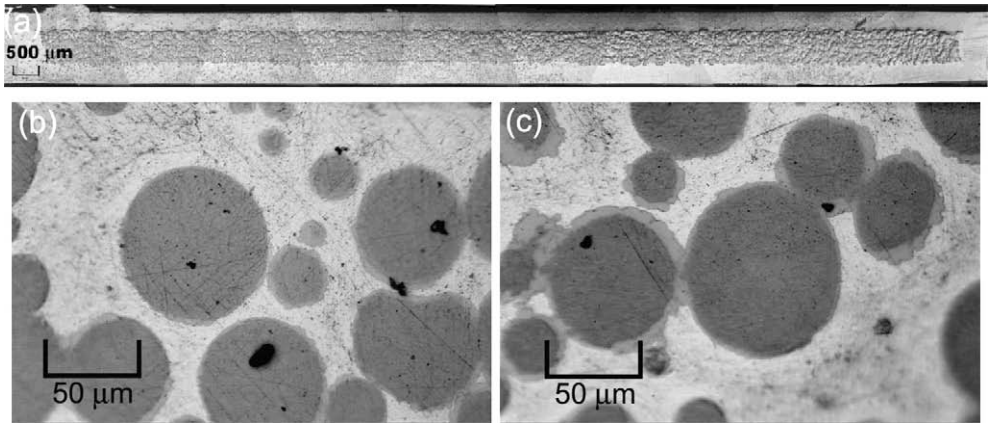


**Fig. 2.** A low magnification optical micrograph (a) of the R2R010 fuel microstructure, where the high-flux side is to the right, and a higher magnification image at the (b) low flux and (c) high-flux side of the fuel plate showing the U–7Mo particles (dark), the Al–2Si matrix (bright), and the interaction layer around fuel particles (medium-gray).

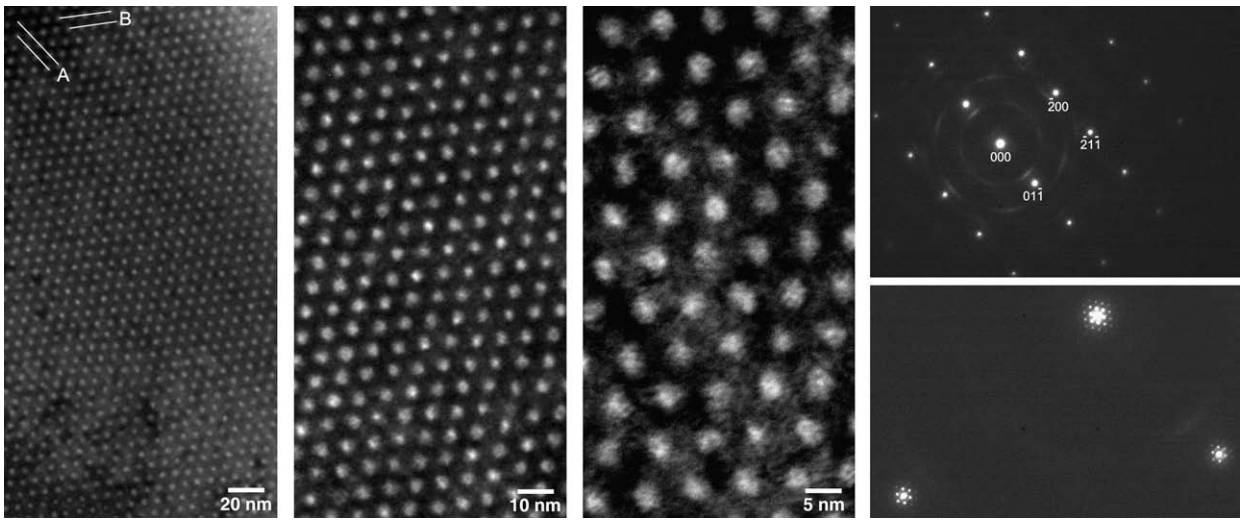


**Fig. 3.** TEM images showing the superlattice of fission gas bubbles observed in a U–7Mo particle of bcc structure orientated at zone [0 1 1]. The selected-area diffraction (SAD) patterns showing rings due to oxides formed at the U–7Mo fuel particle from sample preparation. An enlarged view of the SAD pattern showing the satellite spots due to the bubble superlattice.

SAD pattern are evident. The intensity of the oxide rings varies depending on the location, tilt and orientation of the U–7Mo fuel particle. Morie fringes as a result of surface oxides are visible in the images at high magnification.

Bubble superlattice imaged with U–7Mo oriented at zone [0 0 1] and the SAD pattern showing the corresponding satellite spots are shown in Fig. 4. The plane "C" spacing measured from the bright field image and estimated from the SAD satellite spots are 5.72 nm and 5.53 nm, respectively. The plane spacing measured from bubble images for "A" and "C" is in excellent agreement (5.75 nm vs. 5.72 nm). A final TEM image generated from a U–7Mo particle is presented in Fig. 5 to show some relatively large fission gas bubbles (>100 nm) that were observed in some areas of U–7Mo particles. Based on SEM analysis that has been performed on irradiated RERTR-6 fuel plates, relatively large fission gas bubbles can be observed at the grain boundaries of U–7Mo particles [12].

### 3.2. Characterization of the U–7Mo/matrix interaction layer

A TEM micrograph showing the interaction layer between the Al–2Si matrix and the U–7Mo fuel particle is presented in Fig. 6. The SAD pattern in the inset shows that the interaction layer is amorphous. Measurements of the diffuse ring radii from 10 different locations in the sample indicate an average nearest neighbor distance of approximately 0.251 ± 0.002 nm. Compositional analysis was performed in different areas of the interaction layers to determine the variability of the Si content within the layers. Fig. 7 shows the areas within the interaction layer where compositional analysis was performed, and Tables 1 and 2 enumerate the results of this analysis. From this data, it can be seen that there is fluctuation in the Si content within the interaction layer, along with the U, Mo, and Al. The highest concentrations measured in the interaction layer for U, Mo, Al, and Si were approximately 19, 9, 90, and 12 at.%, respectively. These values appear reasonable regardless of the effect of high radiation background on the EDS detector.

## 4. Discussion

With respect to the observed crystallinity of the γ-phase U–7Mo particles and the presence of an ordered superlattice structure of fission gas bubbles, the TEM characterization results reported in this paper showed good agreement with what was reported for irradiated U–7Mo dispersion fuel samples by Van den Berghe

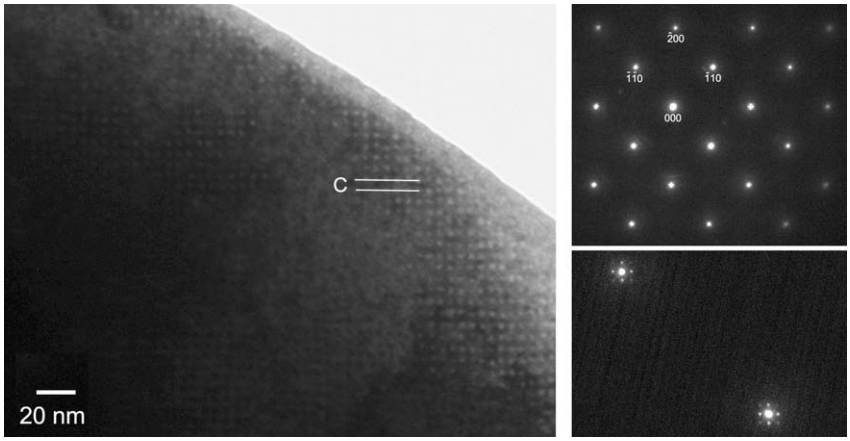


**Fig. 4.** TEM images showing the superlattice of fission gas bubbles observed in U–7Mo fuel particle of bcc structure oriented at zone [0 0 1]. An enlarged view of SAD pattern showing the satellite spots due to fission gas bubble superlattice.


**Fig. 5.** TEM image showing relatively large fission gas bubbles present in a U–7Mo fuel particle.

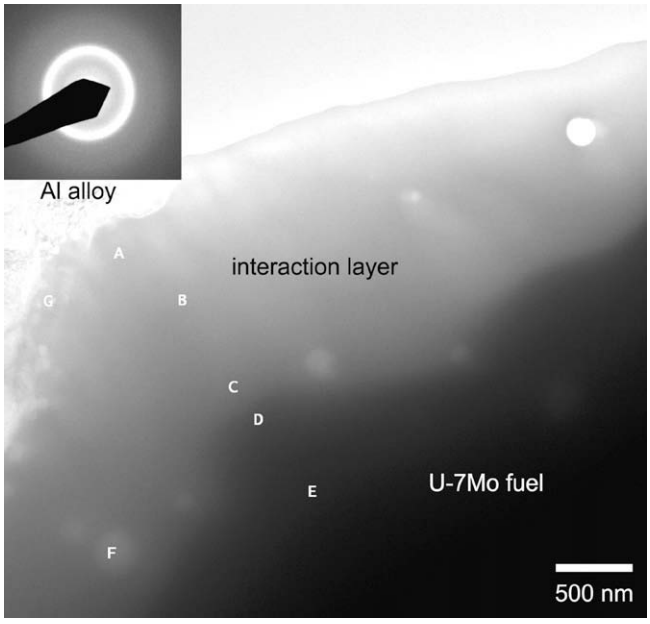


**Fig. 6.** TEM micrograph showing the fuel, interaction layer, and Al alloy matrix with the labels indicating where the EDS measurements were performed (see Table 1). The inset shows the diffraction pattern from the interaction layer demonstrating its fully amorphous character.

et al. [7]. Overall, the U–7Mo remained γ-phase and did not become amorphous during irradiation, and the average size of the fission gas bubbles in bubble superlattice in U–7Mo fuel was ~3.5 nm. The good agreement between the plane spacing measured from bright field image and that estimated from the satellite spots verifies that the observed satellite spots are the result of bubble superlattice that is coherent with U–7Mo bcc structure. The relationship between crystalline orientation of fuel particle, the image of bubble superlattice and the satellite spots from SAD patterns of [0 1 1], [0 0 1] and [1 1 1] indicates that bubble superlattice has a fcc structure oriented parallel to U–7Mo bcc lattice. Bubble superlattice constant is estimated to be ~11.5 nm, two times the plane "A" spacing in Fig. 3. Although radiation-induced superlattices of voids and helium bubbles are observed from many works [13–18], the first observation of a fission gas bubble superlattice was only reported very recently [7].

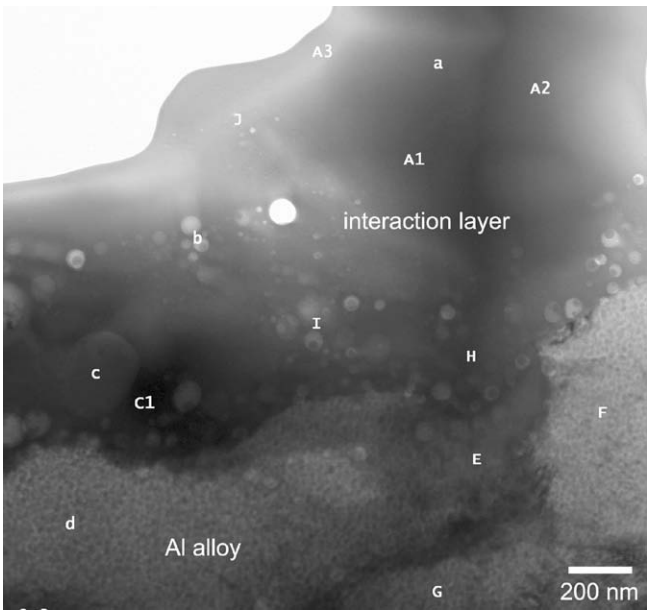


**Fig. 7.** TEM micrograph showing locations near the interface of interaction layer and Al alloy matrix where composition analysis was performed (see Table 2).

**Table 1**
Measured compositions, in at.%, at various locations shown in Fig. 6.

| Spot | Al | Si | Mo | U |
|---|---|---|---|---|
| A | 77.8 | 11.4 | 1.9 | 8.9 |
| B | 66.9 | 12.1 | 4.7 | 16.3 |
| C | 68.7 | 5.1 | 6.9 | 19.3 |
| D | 40.1 | 3.8 | 12.1 | 44.0 |
| E | 20.9 | 0 | 23.9 | 56.7 |
| F | 50.7 | 4.4 | 8.8 | 36.0 |
| G | 84.1 | 7.3 | 0 | 9.7 |
| H | 93.7 | 6.0 | 0 | 0.2 |

**Table 2**
Measured compositions, in at.%, at various locations in the interaction layer shown in Fig. 7. The sign "—"indicates the element is not measured.

| Spot | Al | Si | Mo | U | Zr |
|---|---|---|---|---|---|
| A1 | 78.2 | 9.9 | 2.5 | 9.4 | — |
| A2 | 74.5 | 9.2 | 5.5 | 10.7 | — |
| A3 | 75.4 | 8.9 | 4.8 | 10.9 | — |
| b | 79.6 | 8.4 | 3.0 | 8.9 | — |
| c | 93.8 | 4.7 | 0.7 | 0.7 | — |
| C1 | 85.5 | 5.5 | 3.0 | 3.4 | 2.6 |
| d | 91.2 | 7.2 | 0.7 | 0.2 | 0.8 |
| E | 91.6 | 5.2 | 1.1 | 0.2 | 1.7 |
| F | 91.8 | 6.3 | 0.6 | 0.3 | 1.0 |
| G | 90.6 | 7.8 | 0.6 | 0.2 | 0.8 |
| H | 87.9 | 6.8 | 2.2 | 0.4 | 2.7 |
| I | 89.7 | 5.6 | 2.1 | 2.6 | — |
| J | 82.8 | 4.2 | 3.3 | 9.7 | — |

The concentration of the three-dimensionally ordered fission gas bubbles is estimated to be $2.63 \times 10^{24}$ bubbles/m$^3$ and a volume fraction of approximately 6.0%. Considering the fission density in this work is three times that reported by Van den Berghe et al. [7], the larger bubble size (3.5 nm vs. ~2 nm) and volume fraction (6.0% vs. 1.4%) of the bubble superlattice in this work is likely due to the difference in fission density.

The fission yield of stable Xe and Kr for $^{235}$U in a power reactor fuel is around 0.149 and 0.0356, respectively [19]. From the fission density, the concentration of stable fission gases (Xe and Kr) in this

work is estimated to be $8.3 \times 10^{26}$ atoms/m$^3$. The corresponding atomic fraction of stable fission gas atoms (Xe and Kr) in U–7Mo fuel particle is approximately 1.8 at.%. Assuming that all the Xe and Kr atoms are in bubble superlattice, the average number of gas atoms in a bubble is estimated to be ~316. Under the limiting condition with each fission gas atom occupying a volume of 0.085 nm$^3$ [20], the calculated average bubble diameter in the bubble superlattice is ~3.7 nm. This is in good agreement with the measured 3.5 nm. Considering a significant fraction of the fission gas atoms reside in the relatively large bubbles at grain boundaries, the average number of gas atoms in each bubble in the bubble superlattice should be smaller than what was estimated above. However, the average bubble size in the bubble superlattice is probably close to what was calculated above for the reduced number of gaseous atoms once the volume occupied by a fission gas atom is relaxed from the limiting condition for a real system. The size and spacing of the observed fission gas bubbles in the bubble superlattice are in general agreement with that of a helium bubble superlattice observed in helium-ion irradiated bcc metals [16]. Although both helium and fission gas atoms (Xe and Kr) are inert and insoluble, there are significant differences in atomic mass, size, and possibly diffusion behavior. It is evident from the comparison that bubble ordering in fission gas bubble superlattice observed in this work is much better than that of helium bubble superlattice from helium-ion irradiation of bcc metals. Another major difference is that the fission gas bubble superlattice has a fcc structure while helium gas bubble superlattice has a bcc structure as reported by Johnson et al. [18].

For U–7Mo dispersion fuel, the observed finely distributed bubble superlattice is believed to play an important role in the delay of the breakaway swelling. Fission gas retention in U–7Mo solution or lattice defects is expected to be small due to insolubility of Xe and Kr atoms. The formation of a stable bubble superlattice and a uniform growth of bubble size is probably the most effective mechanism to accommodate production of the insoluble Xe and Kr fission gaseous atoms in the U–7Mo fuel particles without causing severe fuel swelling. Considering bubble superlattice constant is 33.5 times that of U–7Mo bcc structure, the nucleation mechanism for fission gas bubble superlatice is not clear and is expected to be more complex than bubble nucleation. Once nucleated, the bubble superlattice appears stable and bubble size grows as fission density increases. The stable bubble superlattice and lack of bubble coalescence suggest that the surface energy is not a controlling factor in the development of bubble superlattice in U–7Mo fuel particles. It is believed that small bubbles can maintain high gas pressure and store gas more efficiently than large ones [21]. The presence of large fission gas bubbles (>100 nm) in U–7Mo fuel particles, as shown in Fig. 5, suggests that the capacity of fission gas retention in the stable bubble superlattice may be reaching to its limit at the specified fission density. As the fission density further increases, it is anticipated that the large fission bubbles will continue to form and grow while the superlattice structure of fine fission gas bubbles will be destroyed before the interlinking of bubbles occurs. According to a model predication, at around 40–50% $^{235}$U burnup, radiation-induced recrystallization of the U–7Mo fuel is anticipated [22]. If it is true, the recrystallization could affect fission gas bubbles in the fuel particle because of a significant increase in grain boundary interface, redistribution of a fraction of Xe and Kr atoms previously occupied at bubble superlattice to the newly available grain boundaries. A sophisticated modeling of the evolution of bubble superlattice is needed to fully account for the effect of microstructural development on fuel swelling behavior.

The Si-rich interaction layers, that originated between the U–7Mo particles and the Al–2Si matrix during fuel fabrication and contained crystalline phases [23], have become amorphous during irradiation. This is analogous to the irradiated U–7Mo/Al dispersion fuel reported by Van den Berghe et al. [7] where the interaction layer was also found to be amorphous. The estimated average distance of the nearest neighbors from the diffuse ring in Fig. 6 is 0.251 nm, slightly higher than the value of 0.239 nm reported in [7]. The ~5% increase in the average nearest neighbor distance may be related to the cluster expansion by the presence of Si or by the more effective trapping of individual fission gas atoms in the amorphous interaction layer promoted by Si participation.

The EDS measurements from this work and previous work on SEM characterization of the same fuel sample with element mapping indicate the presence of Xe gas in the interaction layers [9]. One speculation is that these fission gases may have been retained in the layer as individual gas atoms or very small fission gas bubbles (<2 nm) up to moderate burnup. For irradiated U–7Mo dispersion fuels with pure Al as the matrix, the fission gases seem to have more of a tendency to migrate through the interaction layer during irradiation to the interaction layer/matrix interface where they can agglomerate into large pores that can ultimately interconnect and cause failure of a fuel plate.

Although EDS signal for a highly radioactive TEM sample has a high background noise, it was found that composition information still can be extracted from this sample of high β-ray and relatively low γ-ray radioactivity. The EDS measurements suggest that the areas of the interaction layers with the fewest observable fission gas bubbles were also the most enriched in Si. The presence of Si in the amorphous interaction layer seems to affect certain properties of the material (e.g., viscosity) such that there is a propensity of the layer to retain the fission gases. Si atoms in the interaction layer may possibly occupy the relatively open volume sites. Another possibility is that Si may enhance the bonds between the atoms in the cluster. Both of these effects are likely to reduce the mobility for fission gas atoms. Hofman and Kim [24] proposes that for U–Si fuels, which also go amorphous during irradiation, the additional Si bonds in $U_3Si_2$ relative to $U_3Si$ results in an improvement in irradiation performance. These additional bonds reportedly have a large effect on the amount of free volume in the material, which affects the diffusion property of the fuel and hence the fission gas diffusivity and swelling behavior. For the $U_3Si_2$, which behaves well during irradiation, the increase in free volume during amorphization is negligibly small, and for $U_3Si$, which behaves poorly during irradiation, the increase in free volume during amorphization is relatively large. This means that just because a material goes amorphous, it is not guaranteed that there will be a large swelling increase unless there is a significant increase in free volume.

The morphology of fission gas bubbles in actual irradiated U–Si fuels has been discussed by Finlay and Leenaers [25,26]. Finlay et al. [25] reports that irradiated USi and $U_3Si_2$ fuels develop a uniform, round, very small fission gas bubble, while $U_3Si$ displays bubbles that have no uniformity and show signs of migration and interlinkage. Leenaers et al. [26] reports that the size of the fission gas bubbles in irradiated U–Si fuels is related to the composition of the fuel particles. Many relatively small (100–300 nm) fission gas bubbles are observed in irradiated USi, while irradiated $U_3Si_2$ has fewer bubbles with areas that contain larger fission gas bubbles (up to 1 μm). The bubbles observed in these two silicide phases were perfectly round and showed no indication of bubble coalescence. However, the $U_3Si$ fuel exhibits unstable fission gas behavior in that the fission gas bubbles grow to several micrometers, vary in shape and show interlinkage [21].

For the case of the Si-containing interaction layers in fuel plate R2R010, the Si may be having a similar effect as it did for the U–Si fuels. For areas of the interaction layers where the Si content is relatively high, the amount of free volume increase is small when

the material goes amorphous during irradiation, and for cases where the Si content is relatively low, the free volume increase is larger and the fission gas bubbles become increasingly mobile and can grow to relatively large sizes. In the R2R010 punchings that were analyzed using SEM [9], it was actually observed that the fission gas bubbles significantly increased in size in some interaction layer regions where the Si concentration was relatively low. This would suggest that the properties of the interaction layer had changed because of the lower amount of Si (perhaps the larger free volume), which probably resulted in a lower viscosity of the amorphous material, an increase in the mobility of fission gases, and an increase in growth of the bubbles. Due to small thickness of interaction layer (typically several micrometers) and the submicron-scale local fluctuation of Si content, nanohardness measurements on the interaction layers of a SEM sample from the same irradiated fuel plate may be needed to verify the Si effect on viscosity.

## 5. Conclusions

Based on TEM characterization of a U–7Mo/Al–2Si dispersion fuel plate irradiated to moderate burnup in the RERTR-6 experiment, the following conclusions can be drawn:

1. U–7Mo fuel particles irradiated to medium burnup retain their crystallinity and contain small fission gas bubbles distributed on a three-dimensionally ordered superlattice. The bubble superlattice has a fcc structure coherent with the U–7Mo bcc lattice.
2. The Si-rich interaction layers, that originally developed around U–7Mo particles during fuel plate fabrication and are present when a fuel plate is inserted into the reactor, become amorphous during irradiation. These layers exhibit stable irradiation behavior.

## US department of energy disclaimer



## Acknowledgments

Acknowledgment is given to the INL Hot Fuel Examination Facility staff for producing the punching sample from fuel plate R2R010. This work was supported by the US Department of Energy, Office of Nuclear Materials Threat Reduction (NA-212), National Nuclear Security Administration, under DOE-NE Idaho Operations Office Contract DE-AC07-05ID14517. Accordingly, the US Government retains a nonexclusive, royalty-free license to publish or reproduce the published form of this contribution, or allow others to do so, for US Government purposes.

## References

[1] M.K. Meyer, G.L. Hofman, S.L. Hayes, C.R. Clark, T.C. Wiencek, J.L. Snelgrove, R.V. Strain, K.H. Kim, J. Nucl. Mater. 304 (2002) 221–236.
[2] F. Mazaudie, C. Proye, F. Hodaj, J. Nucl. Mater. 377 (2008) 476–485.
[3] User Handbook for the Advanced Test Reactor, Idaho National Laboratory, USA, unpublished.
[4] D. Wachs, D. Keiser, M. Meyer, D. Burkes, C. Clark, G. Moore, J. Jue, M. R. Finley, T. Totev, G. Hofman, in: Proc. of GLOBAL 2007, Boise, ID, September 9–13, 2007.
[5] C.R. Clark, S.L. Hayes, M.K. Meyer, G.L. Hofman, J.L. Snelgrove, Transaction of RRFM 2004, Munich, Germany, March 2004, p. 41. <http://www.euronuclear.org/pdf/RRFM-2004-Transactions.pdf>.
[6] H.J. Ryu, J.M. Park, C.K. Kim, Y.S. Kim, G.L. Hofman, J. Phase Equilib. Diffus. 27 (6) (2006) 651–658.
[7] S. Van den Berghe, W. Van Renterghem, A. Leenaers, J. Nucl. Mater. 375 (2008) 340–346.
[8] G.L. Hofman, M.R. Finley, Y.S. Kim, RERTR 2004, Vienna, Austria. <http://www.rertr.anl.gov/RERTR26/pdf/10-Hofman.pdf>.
[9] D.D. Keiser, Jr., A.B. Robinson, J.F. Jue, P. Medvedev, M.R. Finley, in: Proceedings of RRFM 2009, Vienna, Austria, March 23–25, 2009, p. 99. <http://www.euronuclear.org/meetings/rrfm2009/transactions/rrfm09-transactions.pdf>.
[10] Y.S. Kim, H.J. Ryu, G.L. Hofman, S.L. Hayes, M.R. Finley, D.M. Wachs, G.S. Chang, RERTR 2006, Cape Town, South Africa, <http://www.rertr.anl.gov/RERTR28/PDF/S15-1_Kim.pdf>.
[11] J. Gan, D.D. Keiser, D.M. Wachs, B.D. Miller, T.R. Allen., Hot Laboratories and Remote Handling Conference (HOTLAB 2008), Kendal, England, September 22–23, 2008.
[12] D.D. Keiser, Jr., J.F. Jue, J. Gan, A.B. Robinson, B.D. Miller, RERTR 2008, Washington, DC.
[13] K. Krishan, Radiat. Eff. 66 (1982) 121–155.
[14] P.B. Johnson, D.J. Mazey, J. Nucl. Mater. 93–94 (1980) 721–727.
[15] P.B. Johnson, A.L. Malcolm, D.J. Mazey, Nature 329 (September 24) (1987) 316–318.
[16] P.B. Johnson, D.J. Mazey, J. Nucl. Mater. 218 (1995) 273–288.
[17] F.E. Lawson, P.B. Johnson, J. Nucl. Mater. 252 (1998) 34–42.
[18] P.B. Johnson, F.E. Lawson, Nucl. Instrum. Methods Phys. Res., Sect. B 243 (2006) 325–334.
[19] W.J. Maeck, R.M. Abernathy, J.E. Rein, Transactions of the American Nuclear Society, 1965 Annual Meeting, June 21–24, 1965, Gatlinburg, Tennessee, pp. 10–11.
[20] D.R. Olander, Fundamental Aspects of Nuclear Reactor Fuel Elements. US Department of Energy, ISBN: 0870790315, 202.
[21] G.L. Hofman, J. Nucl. Mater. 140 (1986) 256–263.
[22] J. Rest, G.L. Hofman, Y.S. Kim, J. Nucl. Mater. 385 (2009) 563–571.
[23] D.D. Keiser, Jr., J. Gan, J.F. Jue, B.D. Miller, Electron microscopy characterization of an as-fabricated research reactor fuel plate comprised of U–7Mo particles dispersed in an Al–2Si alloy matrix, Materials Characterization, submitted to publication.
[24] G.L. Hofman, Y.S. Kim, Nucl. Eng. Technol. 37 (2005) 299–308.
[25] M.R. Finlay et al., J. Nucl. Mater. 325 (2004) 118–128.
[26] A. Leenaers et al., J. Nucl. Mater. 375 (2008) 243–251.